
Article:
Manian, A., Shaw, R.A. orcid.org/0000-0002-9977-0835, Lyskov, I. et al. (2 more authors) (2021) Modeling radiative and non-radiative pathways at both the Franck–Condon and Herzberg–Teller approximation level. The Journal of Chemical Physics, 155 (5). 054108. ISSN 0021-9606

https://doi.org/10.1063/5.0058643

The Journal of Chemical Physics

Modelling radiative and non-radiative pathways at both the Franck-Condon and Herzberg-Teller approximation level

A. Manian,[1] R. A. Shaw,[2] I. Lyskov,[1] W. Wong,[3,4] and S. P. Russo[1, a)]
[1)]*ARC Centre of Excellence in Exciton Science, School of Science, RMIT Univeristy, Melbourne, 3000, Australia.*
[2)]*Department of Chemistry, University of Sheffield, Sheffield S3 7HF, UK*
[3)]*ARC Centre of Excellence in Exciton Science, School of Chemistry, The University of Melbourne, VIC 3052, Australia.*
[4)]*Australian Centre for Advanced Photovoltaics, School of Chemistry, The University of Melbourne, Parkville, Victoria, 3010, Australia*

(Dated: 15 July 2021)

Here, we present a concise model which can predict the photoluminescent properties of a given compound from first principles, both within and beyond the Franck-Condon approximation. The formalism required to compute fluorescence, Internal Conversion (IC), and Inter-System Crossing (ISC) is discussed. The IC mechanism in particular is a difficult pathway to compute due to difficulties associated with the computation of required bosonic configurations and non-adiabatic coupling elements. Here, we offer a discussion and breakdown on how to model these pathways at the Density Functional Theory (DFT) level, with respect to its computational implementation, strengths and current limitations. The model is then used to compute the photoluminescent quantum yield (PLQY) of a number of small but important compounds: Anthracene, Tetracene, Pentacene, diketo-pyrrolo-pyrrole (DPP), and Perylene Diimide (PDI), within a polarizable continuum model. Rate constants for fluorescence, IC, and ISC compare well for the most part with respect to experiment, despite triplet energies being overestimated to a degree. The resulting PLQYs are promising with respect to the level of theory being DFT. While we obtained a positive result for PDI within the Franck-Condon limit, the other systems require a second order correction. Recomputing quantum yields with Herzberg-Teller terms yields PLQYs of 0.19, 0.08, 0.04, 0.70, and 0.99 for Anthracene, Tetracene, Pentacene, DPP, and PDI respectively. Based on these results, we are confident the presented methodology is sound with respect to the level of quantum chemistry, and presents an important stepping stone in the search for a tool to predict properties of larger, coupled systems.

I. INTRODUCTION

Ab initio modelling of molecular photophysical processes is finding increasing importance in the field of photon harvesting, with applications ranging from organic light emitting diodes[1], to organic photovoltaic devices[2,3], to luminescent solar concentrators[4,5]. Since each device generally relies on one particular de-excitation pathway out-performing others, the ability to predict quantum chemical processes occurring within a given compound pre-device fabrication can expedite the overall process.

One such chemical property is the quantum yield of a compound; a measure of the relative efficiency of a particular pathway across all competing mechanisms. With respect to photon harvesting applications, an important quantum yield type is that of the photoluminescence quantum yield ($Q_x = PLQY$): the probability that a molecule will radiate upon photorelaxation. A quantum yield of any particular process is computed simply as a ratio of the rate of interest k_x, against the sum of all possible mechanism $\sum k$, given simply as:

$$Q_x = \frac{k_x}{\sum k} \tag{1}$$

However, in order to compute a quantum yield, we need both an understanding of the various mechanisms at play belonging to $\sum k$, and an appropriate model which can predict the rate constants for each pathway.

Molecular photophysical processes can be catagorised as either intermolecular or intramolecular. Intermolecular processes occur via coupling between two molecular bodies, facilitating additional decay pathways not normally accessible. These processes are very sensitive to many systemic factors, such as interchromophore separation and spatial geometry or molecular conformation, and have been explored in previous studies[6,7]. Conversely, an intramolecular process is dependant only on a monomer, and is affected only by the immediate surroundings of a given compound, such as a solvent or tightly coupled radical.

The individual processes themselves can be further divided into subcategories: as either radiative, in which relaxation of an exciton results in the emission of a photon, or non-radiative (NR), where energy is released in some form of heat. In terms of intramolecular processes, there are two probable NR pathways we can consider: relaxation via release of heat in which electron spin is conserved, and heat release where spin is *not* conserved. The former is known as internal conversion (IC), mediated by non-adiabatic (vibronic) coupling, while the latter is known as inter-system crossing (ISC), mediated by spin-orbit (SO) coupling[8,9].

The formalism for computing the rate constants for radiative and NR pathways can then be applied at one of two levels: within the Franck-Condon (FC) regime[10–12], and beyond the Franck-Condon regime, also called the Herzberg-Teller (HT) regime[13]. In simple terms, the dependence of the pertur-

[a)]Electronic mail: salvy.russo@rmit.edu.au

bation operator on the nuclear coordinates is omitted within the Franck-Condon regime, while it is considered within the Herzberg-Teller regime. This leads to "intensity borrowing" from the neighbouring states, in that a given Herzberg-Teller contribution is never zero, however its importance is only highlighted for transitions in which the wavefunctions components are heavily mixed, or when excited state manifolds are in close energetic proximity to each other. Good examples include Naphthalene[14] and Psoralen[15], where fluorescence and ISC rate constants were easily underestimated when neglecting the second order terms of the perturbation operator.

While plenty of work has been devoted towards ISC and how to model the mechanism[14–18], IC is significantly more difficult to model, with very few studies having successfully dealt with it[19–23]. *Ab initio* treatments of IC can be tricky due to the difficulties associated with the evaluation of the non-adiabatic coupling term and the required bosonic configurations. In the case of the former, works combining the efforts of Plotnikov, Robinson and Jortner at the INDO level have shown some success in treating this mechanism semiempirically[24–27]. However, the combination of this framework with time-dependent density functional theory (TDDFT) yielded much more accurate rate constant calculations[28–30], which we call the Plotnikov-Robinson-Jortner (PRJ) formalism. However, in the case of the latter bosonic configuration problem, the difficulty boils down to the fact that no known polynomial-time algorithm offers an exact solution[31]. Of course these solutions do exist; one can simply enumerate every possible configuration with respect to some satisfactory condition until a full continuum, or configuration space (CS), is generated. However, as every possible permutation of vibronic transitions must be considered, the number of configurations increases rapidly, therefore the use of such a brute-force methodology to search for energetically accessible configurations quickly becomes intractable.

It should be noted that nowhere else in the literature is a similar bosonic calculation implemented, as this problem is analogous to the 0-1 Knapsack problem in mathematics. Valiev and co-workers[30] have recently discussed a solution to the problem through the use of a Lagrangian multiplier to estimate the most probable vibronic configuration, offering valuable insight into the problem. Here, a similar framework has been implemented. We have recently published a number of viable methods for computation of such bosonic configurations beyond just the maximum[32], and will illustrate how it is employed further in this study, as well as present an open source code which allows for ready replication of our methods. This will be discussed in more detail later.

This paper is organised as follows: Section II presents the underlying theory for our implementation and the expressions used to compute the rate constants in as straight forward a manner as possible. Here, we explain fundamental ideas, as well as illustrate how the CS is generated. We then apply this to a number of example systems. The computational details used are presented in Section III, while Section IV validates the theory and discusses the results. We will then combine all the rate constants within the Franck-Condon and Herzberg-Teller regimes to calculate a fluorescence internal quantum yield for each example system of interest, and compare it with experimental values, and any other similar studies where possible. Section V will then summarise the work, and highlight when the suggested protocol is appropriate for use.

II. THEORY

A. Radiative Decay

The rate of radiative decay k_r is easily calculated as per Einstein's spontaneous emission function[1,33]:

$$k_r = \frac{1}{\tau_r} = \frac{4}{3\hbar c^3} \left\langle \Psi_0 \left| \hat{d} \right| \Psi_1 \right\rangle^2 \int S_d(\omega)\omega^3 d\omega \qquad (2)$$

Here, τ is the fluorescent lifetime, $\hbar$ is Planck's reduced constant, c is the speed of light, S_d is the normalised emission bandshape, and $\left\langle \Psi_0 \left| \hat{d} \right| \Psi_1 \right\rangle$ is the transition dipole moment. These quantities are readily calculated in standard quantum chemistry packages. For convenience, the transition dipole moment is also denoted by μ.

To go beyond the Franck-Condon approximation, the transition dipole can be expanded as a power series with respect to the vibrational coordinates Q_j of the equilibrium geometry Q_0[33]. Truncation of the Taylor expansion after the first-derivative term leads to the following:

$$\mu_\gamma = \mu_{0,\gamma} + \sum_j \left[\frac{\partial \mu_\gamma}{\partial Q_j} \right]_{Q_0} Q_j, \quad \gamma = x,y,z \qquad (3)$$

where the first term on the righthand side mediates the FC contribution to emission bandshape, while the second term mediates the HT contribution.

B. Internal Conversion

The general expression for rate constants using PRJ formalism uses Fermi's Golden Rule[24–26,28] is given in atomic units as:

$$k_{IC} = \sum_n \left| V_{i0,f(n_1 n_2 \ldots n_{3N-6})} \right|^2 \Gamma_{fn} \left[\Delta_{if}^2 + \frac{\Gamma_{fn}^2}{f} \right]^{-1} \qquad (4)$$

Here, Γ_{fn} is the relaxation width of the vibrational level $|fn\rangle$, Δ_{if} is the energy difference between initial and final vibrational states, and $V_{i0,f(n_1 n_2 \ldots n_{3N-6})}$ is the matrix element of the perturbation operator[28]. If we assume that the relaxation width depends only weakly on the vibrational level n, and that the difference in energy of the initial and final vibrational states is much smaller than the relaxation width[24], we can simplify Equation 4 down to:

$$k_{IC} = \frac{4}{\Gamma_f} \sum_{n_1,n_2,\ldots,n_{3N-6}}^{E_{if}=n_1\omega_1+n_2\omega_2+\ldots+n_{3N-6}\omega_{3N-6}} \left| V_{i0,f(n_1 n_2 \ldots n_{3N-6})} \right|^2 \qquad (5)$$

where i and f are the initial and final electronic states, n is the vibrational level of the state, E_{if} is the vertical energy gap

between electronic states as per the Franck-Condon approximation, and ω_j is the frequency of the j^{th} vibrational mode. The CS is scanned by searching for all possible solutions to the summation:

$$E_{if} = n_1\omega_1 + n_2\omega_2 + ... + n_{3N-6}\omega_{3N-6} \tag{6}$$

where n_j is the occupation number of the j^{th} normal mode within a given vibronic configuration. Only configurations inside the CS which satisfy the energy condition E_{if} factor into the rate expression. Computation of the CS is discussed in a following section.

The relaxation width Γ_f can be implemented as a semi-empirical component with a value of approximately 0.16 PHz. However, it can also be computed directly from first principles using the Lax-Pekar model[34,35] and can be expressed in terms of a dispersion parameter, shown in full form as:

$$\Gamma_f = \sqrt{8\ln 2 \sum_{j}^{3N-6} y_j\omega_j^2(2\sigma_j+1)} \tag{7}$$

where y_j is the Huang-Rhys (HR) factor, and σ_j is the average number of particles occupying the j^{th} state. Since we are considering vibrational normal modes, we can use a Bose-Einstein occupancy[34], given by:

$$\sigma_j = \left[e^{\frac{\hbar\omega_j}{k_bT}} - 1\right]^{-1} \tag{8}$$

where k_b is Boltzmann's constant, and T is the temperature. The Huang-Rhys factor is the strength of coupling to the nuclear degrees of freedom, and can be computed from the Franck-Condon factors[35]:

$$y_j = \frac{\nabla^2}{2} \tag{9}$$

where ∇_j is the Franck-Condon displacements of the j^{th} mode in dimensionless normal coordinates.

For the IC mechanism, the perturbation term is expressed in full as:

$$V_{i0,fn} = \langle i|T_r|f\rangle\langle 0|n\rangle - \sum_{\alpha}^{3N}\frac{1}{M_\alpha}\left\langle 0\left|\frac{\partial}{\partial R_\alpha}\right|n\right\rangle\left\langle i\left|\frac{\partial}{\partial R_\alpha}\right|f\right\rangle \tag{10}$$

where T_r is the kinetic energy operator of the electrons, α is a nuclear index, with M_α signifying the mass of nucleus α, $\left\langle i\left|\frac{\partial}{\partial R_\alpha}\right|f\right\rangle$ is the non-adiabatic coupling matrix elements (NACME) between the initial and final electronic states, $|0\rangle$ is the lowest vibrational state of $|i\rangle$, $|n\rangle$ is a given vibrational state of the final electronic state, R_α are the nuclear coordinates of nucleus α, and $\left\langle 0\left|\frac{\partial}{\partial R_\alpha}\right|n\right\rangle$ is the Franck-Condon coupling between $|0\rangle$ and $|n\rangle$. The first term on the right hand side of Equation 10 can be neglected due to it's small size of overlap integrals compared with the second term[24]. We can then express the function using Cartesian coordinates as follows:

$$V_{i0,fn} = -\sum_{q}^{3N}\frac{1}{M_q}\left\langle i\left|\frac{\partial}{\partial R_q}\right|f\right\rangle\left[\sum_{j=1}^{3N-6}B_{qj}\left\langle 0_j\left|\frac{\partial}{\partial Q_j}\right|n_j\right\rangle\prod_{\substack{k\neq j\\k=1}}^{3N-6}\langle 0_k|n_k\rangle\right] \tag{11}$$

where $|0_k\rangle$ and $|n_k\rangle$ are the harmonic oscillator wavefunctions of the initial and final states respectively, and B_{qj} are the matrix elements describing the connection between Cartesian displacement of the q^{th} element with respect to the normal coordinate of the j^{th} element, what we call the internal conversion vibronic matrix (ICV). In other words, the ICV is constructed using the mass weighted normal modes of each vibrational mode participating in the transition, or transition participating modes (TPMs). We can then use the harmonic approximation to express the final few terms[28].

$$\left\langle 0_j\left|\frac{\partial}{\partial Q_j}\right|n_j\right\rangle^2 = \frac{\omega_j}{2n_j!}(n_j-y_j)^2y_j^{n_j-1}e^{-y_j} \tag{12}$$

Each configuration is then weighted against it's relative intensity, obtained from modified Franck-Condon factors computed as:

$$\langle 0_k|n_k\rangle^2 = \frac{e^{-y_k}y_k^{n_k}}{n_k!} \tag{13}$$

To include additional intensity borrowing and go beyond the Franck-Condon approximation, we have to include higher order elements of the power series of the perturbation operator. For this, we consider the full Hessian of the initial singlet excited state in addition to the ICV[30]. Making the same assumptions as per Equation 10, we arrive at:

$$V_{i0,fn} = -\sum_{\substack{j=1\\ j'=1}}^{3N-6} \left\langle 0_j \left| \frac{\partial}{\partial Q_j} \right| n_j \right\rangle \left\langle 0_{j'} \left| Q_{j'} \right| n_{j'} \right\rangle \left[\sum_{\substack{q=1\\ q'=1}}^{3N-6} \frac{B_{qj} B_{q'j'}}{M_q M_{q'}} \left\langle i \left| \frac{\partial^2}{\partial R_q R_{q'}} \right| f \right\rangle \prod_{\substack{k\neq j\\ k\neq j'\\ k=1}}^{3N-6} \langle 0_k | n_k \rangle \right] \tag{14}$$

where $\left\langle i \left| \frac{\partial^2}{\partial R_q R_{q'}} \right| f \right\rangle$ is the second order term of the expanded NACME (the Hessian), and $\left\langle 0_{j'} \left| Q_{j'} \right| n_{j'} \right\rangle$ is the Herzberg-Teller coupling term, given as:

$$\left\langle 0_{j'} \left| Q_{j'} \right| n_{j'} \right\rangle^2 = \frac{1}{2\omega_j n_j!} (n_j + y_j)^2 e^{-y_j} y_j^{n_j - 1} \tag{15}$$

It should be noted that since the perturbation operator is only dependant on vibrational modes with non-zero HR factors, the CS can be simplified to only consider TPMs.

C. Intersystem Crossing

The rate of ISC is dependant on the magnitude of the spin-orbit coupling matrix element. Here, the perturbation operator is constructed in terms of the spin-orbit coupling matrix element weighed against the Franck-Condon factors:

$$k_{ISC} = \frac{2\pi}{\hbar} \left\langle i \left| \hat{H}_{SO} \right| f \right\rangle^2 \delta(E) \tag{16}$$

Here, $\left\langle i \left| \hat{H}_{SO} \right| f \right\rangle$ is the spin-orbit coupling matrix element, while $\delta(E)$ is the density of states. For convenience, we also denote the spin-orbit coupling term using χ.

In this work, the SOCME is computed using Breit-Pauli Hamiltonians[36], which consists of one-electron and two electron components. This can be simplified by employing a spin-orbit mean field approximation[37], whereby the two-electron component is modelled as a screening potential as a function of their spatial atomic orbitals and average occupation within those orbitals. See Refs 37 and 36 for further details.

To account for HT effects, we expanded the SOCME term using a power series, as similar to what was done for the radiative rate.

III. COMPUTATIONAL METHODS

A. Studied Chromophores

The theory highlighted in the previous section has been applied to a number of organic chromophores, including Anthracene, Tetracene, Pentacene, diketo-pyrrolo-pyrrole (DPP), and Perylene Diimide (PDI). As shown in Figure 1, the Polyacenes[9,14,38–42] are very well studied in literature, and as such provide a good case of validity with respect to the accuracy of a model. DPP is a relatively new chromophore of interest[43–47] due to its extreme tunability, while PDIs[5,7] are important in the field of OLEDs and LSCs, typically displaying large PLQYs.

B. Quantum Chemistry

Molecular geometries of the S_0 state were optimised at the DFT level, using the Becke 3-parameter Lee–Yang–Parr exchange-correlation hybrid functional[48] using the redefined valence triple-zeta polarization basis set def2-TZVP[49] basis set for the Polyacenes and DPP, while for PDI the smaller TZVP basis set was used, as implemented in the GAUSSIAN16 software package[50]. Optimisation of electronically excited equilibrium geometries utilised TDDFT, with the same functionals and basis sets used for ground state calculations. To simulate experimental setups, solvation effects are simulated via the employment of a polarizable continuum model (PCM). CycloHexane is used for the polyacenes due to its weak dispersive interaction with aromatic molecules, especially since the larger polyacenes have some solubility issues[14]. DiMethyl Sulfoxide is used for DPP, as it is solvatochromic in nature[51], and therefore requires a highly polar solvent, while Toluene is used for PDI, as it is non-polar and also minimised interchromophore coupling in experimental solution[52].

The electronic Hessian with respect to nuclear coordinates of the converged geometry was computed. The same functionals and basis sets as per the geometry optimisations are employed. The output is in dimensionless normal coordinates, so the ICV was then mass weighted and renormalised. The NACME terms were computed at the first singlet excited state using GAUSSIAN16.

Single-point calculations of optimised structures were performed using the DFT based multireference configuration interaction DFT/MRCI method[53], using the def2-TZVP basis set for all five chromophores. Computed energies using the DFT/MRCI protocol have been shown to display a minimal deviation from experimental results by less than 0.2 eV[53], allowing for significantly more accurate results than typical TDDFT correlated energies. For each chromophore, the one-particle basis was computed using the Becke half-and-half Yang-Lee-Parr BHLYP exchange-correlation functional[54] as implemented in the TURBOMOLE software package[55]. Here, the PCM was employed using the COSMO module[56]. The DFT/MRCI reference space was generated iteratively by including all electron configurations with expansion coefficients greater than 10^{-3} in numerous probe calculations, using 10 electrons across 10 orbitals, allowing only for a maximum of two-electron excitations. Probe runs were calculated by discarding configurations with energy less than the highest reference energy; starting with a threshold of $0.6E_h$, then 0.8, with the finalised wavefunction built using a threshold of 1.0. Molecular orbitals with energies larger than 2.0 E_h were not used. Vertical excitation energies and transi-

FIG. 1. Schematic molecular structures of studied compounds.

tion dipole moments can be extracted from these results. Spin-orbit matrix elements were computed using the SPOCK.CI module[36,37,57] of the DFT/MRCI platform.

The transition dipole moment and spin-orbit coupling matrix element is defined as:

$$\langle i|\hat{V}|f\rangle = \sqrt{\sum_{\gamma=x,y,z} \left|\langle i|\hat{V}|f_\gamma\rangle\right|^2} \tag{17}$$

where subindex γ defines the perturbation interaction V across the singlet/triplet sublevels. Here, any triplet state with energy in close energetic proximity to and all below the first singlet state are considered important to quenching pathways. The VIBES software package[17] was used to compute ISC rates.

VIBES was also used to generate the Franck-Condon and Herzberg-Teller emission spectra, requiring the adiabatic energy of the transition, frequency calculations, and the transition dipole moment. The Franck-Condon factors are obtained from this output. It should be noted that temperature has a

strong effect on the spectra, due to changes in the Boltzmann distribution. As such, all spectra are computed using a temperature of 300 K.

When computing the Herzberg-Teller emission rate, care must be taken as the spectral intensity is unknown. At the Franck-Condon point, this intensity scaling is proportional to the transition dipole moment. However, the Herzberg-Teller treatment mediates an effective transition dipole moment due to nuclear activity of normal modes. Since VIBES computes the spectra in the time domain, this information is not readily accessible. As such, when computing the Herzberg-Teller rate constant as per Equations 2 and 3, the spectra were normalised to the Franck-Condon spectral density.

C. Configuration Space Computation

The last step needed here is to find some appropriate method of computing the CS. As per Equation 6, this is constructed as a function of the electronic energy difference, and the harmonic energies with various occupational quanta within each TPM. Further, the entire CS must be scanned for all configurations which may satisfy the energy condition. However, in its current form, the energy condition is exact. Realistically, this cannot be the case. Vibrational energies fluctuate, and the atoms themselves vibrate, resulting in a small range of energies to sum over. To factor this quality, we modify the energy condition as follows:

$$E_{if} = \sum_{i=1}^{3N-6} n_i\omega_i \pm \delta E \tag{18}$$

where δE is the allowable energy tolerance. It is plausible to infer that this average range of energies can be directly related to the ensemble thermal energy of the system. If we also invoke Boltzmann's constant within a three dimensional system, we arrive at:

$$\delta E = \frac{3}{2}k_B T \tag{19}$$

which relates δE directly to the average thermal energy of a molecule. Here, we employ an energy window of $\delta E = 40meV$, which corresponds to standard room temperature. See the SI for further details with respect to this choice.

As previously mentioned, scanning over the CS is analogous to the 0-1 Knapsack problem in mathematics, and is therefore an NP-complete problem. Ref.[32] outlines three possible solutions. The first is a brute force scan; testing every plausible configuration within the CS. While generating an exact set of solutions, the brute force method is impractical as the total number of possible configurations $\bar{C}$ scales factorially with the number of TPMs. The second method was to stochastically generate configurations, but we observed the number of acceptable configurations for a given system was typically within 3-4 orders of magnitude of $\bar{C}$; while an improvement, can still be intractable for large systems. The third method of CS generation is more elegant, and expand through the CS linearly, hereafter called the Linearly Expanded CS (LeCS) method. Here, a Lagrangian is used to estimate the maximum occupation:

$$\mathscr{L} = ln\left[\prod_{k\neq j,k=1}^{3N-6}\langle 0_k|n_k\rangle\right] - \lambda\left[\sum_{k=1}^{3N-6} n_k\omega_k - E_{if}\right] \tag{20}$$

in a similar way to that of Valiev and co-workers[30], where λ is the Lagrange multiplier, rounding to the nearest integer, since the solution is rarely discrete. We can then expand about this maximum, computationally shifting the problem to a polynomial series. If one were to imagine the full CS as an N-Dimensional surface, one dimension for each TPM, with the "vertical" axis a measure of the rate constant at that configuration, the integration of such a surface would yield the overall rate constant for the transition. Using the LeCS method, the CS surface is simplified to a two dimensional surface, as function of the norm of each configuration vector (index), allowing a truncation to exclude indexes with minimal contributions. A full treatment can be found in Ref 32.

Since the PRJ formalism assumes purely harmonic transitions, to obtain the HR factors for an IC calculation, the initial and final vibrational states uses the ground state results[28]. The resulting HR factors and their corresponding energies have been reported within the SI. Scanning of the CS and computation of the IC rate constant was performed using the Knapsack software package[32].

D. Derivatives & Wavefunction Phase

It should be noted that the Herzberg-Teller terms of an operator can be approximated using vibronic coupling between two excited states in conjunction with CI based methods[58]. However, within the TDDFT regime, this process is much more complex, and is typically presented as a ground-excited state coupling term. As such, this method remains locked out using DFT based methods, requiring the computation of derivative components.

The derivatives of a quantum chemical term at the Franck-Condon point, in this case either the transition dipole moment or the SOCME, can be approximated using a finite differences method. Here, we have opted for a central point difference between Q_0 and Q_j, given as:

$$\frac{\partial V_{j,\gamma}}{\partial Q_j} \approx \frac{V_{j,\gamma}(x+h) - V_{j,\gamma}(x-h)}{2\Delta h} \tag{21}$$

where $V_{j,\gamma}(x+h)$ and $V_{j,\gamma}(x-h)$ are the coupling terms perturbed along the j^{th} normal mode by some increment, in the positive and negative directions respectively, and Δh is the increment value, or step size. Here, we have used a step size of 0.05. In other words, the gradient is calculated as the coupling difference between the positively and negatively stepped perturbation along each given normal mode.

Following a given derivative calculation, attention needs to be paid to the sign of the derivative. In particular, phase shifts can occur during single point calculations of the DFT/MRCI wavefunction components, in which one or all wavefunction

components experiences a phase shift from positive to negative or *vice versa*. Further, the amplitudes of the molecular orbitals can sometimes experience a phase shift, which can be difficult to notice. While it is entirely likely a true sign change may take place, they each need to be checked beyond the point of superficiality.

To circumvent this problem, we constructed a fictitious dot product made using the configuration amplitudes of the leading configurations of the two coupled states. These configuration amplitudes were further multiplied by the largest MO coefficient of the underlying orbitals, to account for orbital rotation. We compare the resulting product to that at the displaced geometries, using the FC point as a reference. If the sign of one of the dot products is altered in this process, interpreted as a change in phase, the appropriate coupling magnitude renormalized by a factor of -1. This ensures that a coupling derivative along a particular vibrational coordinate is obtained consistently with the sign of the FC displacement.

IV. RESULTS & DISCUSSION

A. Quantum Chemical Analysis

The vertical excitation energies and frontier orbitals of the five compounds can be found in the Supplementary Information, while comparisons of singlet energies and a summary of their computed qualities of importance can be found in Tables I and II respectively.

Beginning with the polyacenes, computed properties compare well with those found experimentally[14], while analysis of the electronic structures correlates well with similar studies within the literature[39,78,85]. The highest occupied molecular orbitals (HOMO) and lowest unoccupied molecular orbitals (LUMO) comprising the wavefunctions of the first electronic excited state of Anthracene displays a HOMO→LUMO type character across all geometries. This state was found adiabatically at 3.18 eV and appears bright, with a sizable oscillator strength of 0.125 at the singlet excited state geometry. The dark S_2 state appears across all geometries as an evenly mixed HOMO-1→LUMO and HOMO→LUMO+1 transition. In the triplet manifold, we see that the first excited T_1 state appears as a HOMO→LUMO transition, with wavefunction components becoming steadily mixed in appearance as you proceed to higher energy levels. We also note a near-degeneracy between the S_1 state and T_2 state, as shown in Table II, likely facilitating a fast ISC mechanism. Comparison of these results to CASSCF calculations performed by Kawashima and coworkers appear agreeable, with both configuration state functions and state energies matching well between datasets[39].

Onward to Tetracene, which also compared very well to data published by Kawashima and coworkers[39], strongly agreeing with both the predicted HOMO→LUMO character for the bright S_1 state appearing adiabatically at 2.44 eV, then the mixed HOMO-1→LUMO and HOMO→LUMO+1 character for the S_2 state at the ground state optimised geometry. While the S_1 state character, with an oscillator strength of 1.000, was universal across all geometries, the S_2 state shifted to a doubly excited state HOMO^2→LUMO^2 character when the chromophore was photoexcited. This suggests that at the ground state geometry, a flipping of roots occurs upon photoexcitation, with the higher order doubly excited state swapping positions with the mixed state. In the triplet manifold, the first triplet state appears as a strong HOMO→LUMO transition, with all higher lying states appearing as strongly mixed valence orbitals. We also note another near degeneracy condition between the S_1 and T_2 state.

Pentacene also compares well to literature data sets[78,85]. Here unlike Tetracene, the bright S_1 HOMO→LUMO character and S_2 HOMO^2 →LUMO^2 characters are universal across all geometries, with no root flipping observed. The S_1 state can be found adiabatically at 1.92 eV, with an oscillator strength of 0.083. In the triplet manifold, we again see a T_1 state with a HOMO→LUMO character, with higher lying stated appearing heavily mixed. We also again note a near degeneracy between the S_1 and T_2 states. Observed across all polyacenes, this state is likely very important for ISC pathways as a fast deexcitation pathway.

The polyacenes all yield very similar photophysical properties. Here, we note transition dipole moments akin across all systems, deviating from an average value of 1.33 au by no more than 0.02 au. Even mixing of configuration state functions can be seen on the S_2 state across all polyacenes. We also note adequate vertical spacing between excited states by 0.48 eV, 0.64 eV, and 0.47 eV for Anthracene, Tetracene, and Pentacene respectively. In addition to the minimal sharing of oscillator strength, this suggests that in the radiative scheme, Herzberg-Teller processes do not play a dominating role. We also see very small spin-orbit coupling terms at the Franck-Condon point, with the only sizable term belonging to the endothermic T_3 state in Anthracene, appearing 0.40 eV above the singlet S_1 excited state. However, a number of these triplet levels appear closely packed together, so it can be expected that higher order processes contribute very strongly to transfer mechanisms.

As shown in recent studies[44,46,51,86], the photophysical properties of DPP are incredibly sensitive to the sidegroups attached to the chomophore, in some cases, stabilising in energy by more than 1.0 eV. Since DPP has only recently come into light as an interesting compound for application of fluorescence technologies, comparison of the core chromophore with studies in the literature is difficult, as the physics revolves around it's derivatives. However, from what can be found, comparisons of the electronic structure to the compound's derivatives[87] seem to be very positive. At the ground state geometry, the S_1 HOMO→LUMO orbital is observed as dominant, followed by a HOMO-1→LUMO transition to the S_2 state. Solvation results in the destabilisation of the longitudinal L_b state, placing the transient L_a state lower both vertically and adiabatically at 3.35 eV, with a strong oscillator strength of 0.338. In the triplet manifold, three low-lying states were observed to display non-zero spin-orbit coupling terms. While the T_1 and T_2 coupling terms were small, at 0.014 cm^{-1} and 0.001 cm^{-1}, the T_3 state displayed a very large coupling strength, of 28.373 cm^{-1}.

Properties for PDI agree very well with results published

TABLE I. Tabulated singlet and triplet energies for all studied chromophores computed in this study compared to similar theoretical studies and experimental values. Given absorption $S_0 \rightarrow X$ and emission $S_0 \leftarrow X$ energies are vertical from the ground and the X^{th} excited state respectively, while adiabatic $S_0 \rightsquigarrow X$ energies here are presented as 0-0 transitions. All energies are in units of eV, while a "-" indicates that the information could not be found.

Chromophore	DFT/MRCI			Exp.			Theory		
X=State	$S_0 \rightarrow X$	$S_0 \leftarrow X$	$S_0 \rightsquigarrow X$	$S_1 \rightarrow X$	$S_0 \leftarrow X$	$S_0 \rightsquigarrow X$	$S_1 \rightarrow X$	$S_0 \leftarrow X$	$S_0 \rightsquigarrow X$
Anthracene									
S_1	3.39	2.96	3.18	3.31[a]	3.23[b], 3.30[c]	3.43[d], 3.38[e]	3.40[f]	3.27[g], 3.01[h]	3.43[h], 2.67[i]
S_2	3.61	3.41	3.53	3.45[j]	-	-	3.23[f]	3.66[h]	-
T_1	2.04	1.30	1.77	-	-	1.85[k], 1.82[l]	2.00[f], 1.66[m]	-	-
T_2	3.41	2.92	3.19	-	-	-	3.30[f], 2.84[m]	-	2.40[n]
T_3	3.42	3.37	3.58	-	-	-	3.35[f], 3.50[m]	-	3.77[n]
Tetracene									
S_1	2.61	2.28	2.44	2.60[o]	2.60[p]	2.71[e]	2.80[f], 2.74[q], 2.64[r]	2.63[g], 2.30[s]	-
S_2	3.24	3.08	3.18	3.14[o]	-	-	2.92[f], 3.22[q], 3.48[r]	-	-
T_1	1.38	0.62	1.36	-	-	1.28[k]	1.51[f]	-	1.10[n], 1.25[t]
T_2	2.63	2.25	2.25	-	-	-	2.43[f], 1.87[m]	-	2.58[n]
Pentacene									
S_1	2.06	1.81	1.92	2.31[u]	2.31[v], 2.32[w]	2.12[x]	2.13[y]	1.83[s]	1.61[z]
S_2	2.76	2.34	2.44	2.88[o]	-	-	2.88[aa]	-	2.57[x]
T_1	0.92	0.46	0.73	-	-	0.78[k], 0.83[bb]	-	0.79[g]	-
T_2	2.01	1.70	1.86	-	-	1.67[k]	-	-	-
DPP									
S_1	3.49	3.17	3.35	2.48-3.10[cc]	2.07-2.48[cc]	-	3.11[dd]	-	-
S_2	3.78	-	-	-	-	-	-	-	-
T_1	1.78	1.54	1.83	-	-	1.21[ee]	-	-	-
T_2	3.57	3.15	3.43	-	-	-	-	-	-
T_3	3.92	3.40	3.73	-	-	-	-	-	-
PDI									
S_1	2.36	2.09	2.23	2.35[ff], 2.37[gg]	2.08[ff], 2.34[gg]	2.32[gg]	2.30[hh]	2.05[hh]	2.16[hh]
S_2	3.12	-	-	-	-	-	-	-	-
T_1	1.37	1.01	1.26	-	-	-	-	-	1.15[ii]
T_2	2.68	2.45	2.65	-	-	-	-	-	2.59[ii]

[a]From Ref. 59 using h-heptane. [b]From Ref. 60 using ChloroBenzene. [c]From Ref. 61 using CycloHexane. [d]From Ref. 62 in the vapour phase. [e]From Ref. 38 in the gas phase. [f]From Ref. 39 using MRMP. [g]From Ref. 63 using SCFMO. [h]From Ref. 64 using SAC-CI. [i]From Ref. 65 using TDDFT. [j]From Ref. 66 using CycloHexane. [k]From Ref. 67. [l]From Ref. 68 in Ammonia. [m]From Ref. 69 using CI. [n]From Ref. 40 in alcohol. [o]From Ref. 14 using CycloHexane. [p]From Ref. 70 using Toluene. [q]From Ref. 71 using DFT/MRCI. [r]From Ref. 41 using TDDFT. [s]From Ref. 72 using RAS-2SF. [t]From Ref. 73 in the vapour phase. [u]From Ref. 74 in the gas phase. [v]From Ref. 75 in the gas phase. [w]From Ref. 74 in the vapour phase. [x]From Ref. 76 in n-alkanes and AM1. [y]From Ref. 77 using MRMP. [z]From Ref. 65 using DFTB. [aa]From Ref. 78 using CASPT2/SA-CASSCF. [bb]From Ref. 42 in the vapour phase. [cc]From Ref. 44 using various solvents. [dd]From Ref. 79 using TDDFT. [ee]From Ref. 80 at the TDDFT level. [ff]From Ref. 81 using DiChloroMethane and TDDFT. [gg]From Ref. 82. [hh]From Ref. 83 using TDDFT. [ii]From Ref. 84 using TDDFT.

in literature by Meftahi and co-workers[7] and Yang & Jang[83]. PDI was found to display large energetic spacing between the singly excited HOMO→LUMO bright S_1 state and the heavily mixed S_2 state across all geometries. Here, the calculated adiabatic energy of 2.23 eV compares with 2.28 eV noted by Zhang and coworkers[5], along with the large oscillator strength of 0.82. Within the triplet manifold, the T_1 and T_2 states appear as a HOMO→LUMO and a heavily mixed valence state across all geometries. We also note large energetic spacing between the first and second triplet energy levels. Here, a modest SOCME of 0.75 cm^{-1} and a smaller 0.09 cm^{-1} was found for both levels respectively.

While singlet energies seem to match up well with respect to the expected 0.20 eV error associated with the DFT/MRCI methodology[53], as per Table I, computed triplet energies seem to be generally overestimated. Comparison of literature energies for polyacenes[88] show strong agreement with the first triplet level to literature values. However, the near degeneracy condition for the S_1 and T_2 states for all polyacenes is not noted for any system. The closest seen is for Tetracene, with an S_1 to T_2 experimental gap of 0.05 eV. For DPP, as the molecule is relatively new with respect to the literature, triplet energies for the higher lying states of the core chromophore was difficult to obtain. The value found for the first triplet level does not compare well to the computed value, however, this can easily be attributed to the difference in structures. For PDI, the observed differences in energies are smaller than for other chromophores, but still larger than 0.20 eV. These inaccuracies are likely to result in overestimated ISC rate constants. The symmetry rules for ISC rates can also be consid-

TABLE II. Tabulated singlet to triplet quantum chemical transition properties for all studied chromophores at the Franck-Condon point. Given energies are adiabatic, with negative energy differences being defined as a transition to an adiabatically higher state. Energies are given in units of eV, while SOCME terms are in units of cm^{-1}.

Compound	State	$\Delta E_{S_1 \rightarrow T_n}$	$H_{SO}(x)$	$H_{SO}(y)$	$H_{SO}(z)$
Anthracene	T_1	1.412	-0.00006	0.00001	-0.00002
	T_2	-0.009	-0.00004	-0.00001	0.00000
	T_3	-0.396	-0.00036	-0.00015	0.00527
Tetracene	T_1	1.073	0.00000	0.00003	-0.00001
	T_2	-0.014	0.00001	-0.00005	-0.00002
Pentacene	T_1	1.194	0.00000	-0.00003	0.00000
	T_2	0.059	-0.00000	-0.00007	0.00001
DPP	T_1	1.518	0.00055	0.00036	0.01399
	T_2	-0.077	0.00059	-0.00015	-0.00001
	T_3	-0.380	20.81360	19.28235	0.00079
PDI	T_1	0.973	0.00000	-0.00001	-0.75078
	T_2	-0.416	-0.00430	0.09157	0.00024

ered here, whereby for all five of the studies chromophores, the S_1 and T_1 states share the same character. Under these conditions, the pathway is forbidden. As such, for calculations not implementing symmetry, rate constants may be non-zero, but small.

B. Radiative Decay

Computed emission bandshapes agree well with those found experimentally. The vibronic progression of Anthracene, shown in Figure 2A was found to yield 4 peaks of importance, with a small peak attached to the first, using either first and second order treatments. Interestingly, the experimental spectra shows the second peak to be slightly larger than the first[89], while here the first peak is largest. This is likely caused by solution based effects, such as aggregation induced stabilisation of excited state energies, but it is difficult to say. Tetracene, shown in Figure 2B, displays a steady progression of three smoothly shrinking peaks, agreeing well to experimental spectra[70]. Here we see that difference between first and second order corrected spectra are minimal, with some intensity increase on the secondary and tertiary peaks. Pentacene is also relatively normal with respect to changes between first and second order bandshapes, as seen in Figure 2C. Similar to the previous Polyacenes, we see very little differences, with secondary and tertiary peaks of the second order correction possessing a slightly higher intensity, comparing well to experimental results[14].

Compared to a very similar derivative prepared by Grzybowski & Gryki[46], the computed spectra for DPP, shown in Figure 2D, displays significantly more vibronic detail, with 5 evident peaks, however that can easily be attributed to experimental broadening. As per the cited compound appearing lower in energy by more than 1.0 eV, this is attributed to the phenyl groups opposite each oxygen atom. Shown by Pun, Campos & Congreave[47], the emission bandstructure of DPP is very sensitive to it's side group substituents, so the energetic position can change drastically. However, comparison of multiple sources shows very similar emission spectra[45,90]. Similarly, for PDI, the emission spectra compares very well to that found in literature[5,89]. As shown in Figure 2E, two large peaks can be observed, under both first order and second order approximations, with very little change between them. For these two molecules, we can expect little to no dependence on the second order correction. Interestingly in the case of PDI, we see a slight loss in spectral intensity with respect to the first and second peaks. At the first peak, the first order Franck-Condon treatment yeilds the most intense peak, while for secondary and tertiary peaks, the second order corrected Herzberg-Teller spectra displays a higher intensity.

TABLE III. Computed radiative decay rates of just the Franck-Condon terms, and the second order corrected rate. Fluorescent lifetimes are second order corrected and are compared to literature. Rates and lifetimes are given in units of s^{-1} and ns respectively.

Chromophore	$k_{r,FC}$	$k_{r,FC+HT}$	τ_r (Calc.)	τ_r (Exp.)
Anthracene	4.281×10^7	4.829×10^7	20.7	16.2[a]
Tetracene	2.010×10^7	2.263×10^7	44.2	28.6[a]
Pentacene	9.736×10^6	1.091×10^7	91.7	83.3[a]
DPP	1.220×10^8	1.223×10^8	8.2	5.2-6.1[b]
PDI	1.513×10^8	1.505×10^8	6.6	4.00[c]

[a]From Ref. 14 using Cyclohexane. [b]From Ref. 51 using various solvents. [c]From Ref. 5 using poly(methyl methacrylate).

The Polyacenes were observed to possess a very small number of non-zero Franck-Condon factors due to their high degree of molecular symmetry, and as such displays a very distinct vibronic progressions. PDI on the other hand, displays many non-zero Franck-Condon factors, displaying a strongly defined band structure. Comparison of the structure and bandshape to the simpler Perylene derivative shown by Xiong and co-workers[91] suggests that the imide moities smooth out the vibronic structure, resulting in more well defined features. It also explains why the fluorescent lifetime of the compounds remain roughly universal in experiments with respect to the complexity of the side groups attached to the chromophore[5]. This is also likely why the bandstructure of DPP is so vivid.

The calculated fluorescence rate constants are presented in Table III. For Anthracene, we see a first order rate constant of 4.28×10^7 s^{-1}, corresponding to a fluorescence lifetime of 21 ns. While this approximately 7 ns too fast as per the expected lifetime[14], a second order correction yields a new transition dipole moment of 1.40, with a corresponding rate and lifetime of 4.83×10^7 s^{-1} and 21 ns. A similar qualitative improvement is seen for both Tetracene and Pentacene, with first order rates and lifetimes of 2.01×10^7 s^{-1} and 50 ns, and 9.74×10^6 s^{-1} and 103 ns for respectively, improved by a second order correction to 2.26×10^7 s^{-1} and 44 ns, and 1.09×10^7 s^{-1} and 92 ns respectively. Rate constants for DPP and PDI were significantly less dependent on second order processes, as observed in their emission spectra. Here, the gain in fluorescence is less than 5% for both systems, yielding almost identical first and second order rate constants of 1.22×10^8 s^{-1} for DPP, and 1.51×10^8 s^{-1} for PDI. This

FIG. 2. Calculated emission spectra of Anthracene (A), Tetracene (B), and Pentacene (C) in Cyclohexane, DPP (D) in DiMethylSulfoxide, and PDI (E) in Toluene. Solvents were simulated via a PCM at both the Franck-Condon (Red) and Herzberg-Teller (Blue) levels. Spectra are normalised by intensity, and as such are not to scale.

results in similar fluorescent lifetimes, of 8.2 ns and 6.6 ns for DPP and PDI respectively, which both compare reasonably well with experimental values. Interestingly, PDI is the only studied system which seems to lose spectral intensity with a second order correction, likely caused by a net negative change in the derivative components of the perturbation operation. With a reduction in the rate constant of 8.62×10^5 s^{-1}, this implies a dark state in close proximity to the emitting state, which was already highlighted.

Overall, we see using our method of radiative rate computation yields fluorescence lifetimes in very close agreement with experimental values, as highlighted in Table III. With the exception of Pentacene, which underestimated the lifetime, each lifetime was slightly overestimated, but remained

TABLE IV. Tabulated IC rate constants and *ab initio* linewidths for all studied chromophores. Both linearly expanded configuration space (LeCS) and Lagrangian rate constants are presented for comparison, in addition to both Franck-Condon and Herzberg-Teller components, the range (minimum value to maximum value) of the CS index for computed rate constants, and expected the Lagrangian maximum within the CS. Rate constants are given in units are in s^{-1}.

			Linearly Expanded Configuration Space			Lagrangian Configuration Space		
Chromophore	TPMs	Γ_f (PHz)	Index Range	$k_{IC,FC}$	$k_{IC,HT}$	$\mathscr{L}_{max}$	$k_{IC,FC}$	$k_{IC,HT}$
Anthracene	12	0.113	8/19	2.716×10^2	3.690×10^6	16.67	2.423×10^3	1.240×10^3
Tetracene	15	0.099	6/19	1.741×10^5	2.599×10^7	13.19	6.134×10^2	6.824×10^3
Pentacene	24	0.044	4/16	1.057×10^4	4.698×10^6	5.78	2.826×10^4	1.773×10^7
DPP	13	0.104	4/16	2.785×10^6	4.274×10^3	12.78	6.599×10^6	4.894×10^3
PDI	53	0.081	5/12	3.157×10^3	5.885×10^{10}	8.39	8.006×10^0	1.344×10^6

within a reasonable degree of error to the expected values. Our presented methodology can approximate the second order correction to fluorescence assuming that the Herzberg-Teller term is not dominant. In the case where the second order component is very large, then it falls to reason that the approximation used here would fall short, and severely overestimate the rate constant.

C. Internal Conversion

While the optimised Lagrangian does present a configuration vector size with a maximised rate constant, we find that the resultant rate constant in the integration picture should be treated with some scepticism. On the one hand, should the CS be built of a large number of TPMs, the Lagrangian rate can be underestimated. On the other hand, should the CS be built of a small number of TPMs, the Lagrangian rate can be overestimated. The rounding from the Lagrangian result may be too far in a particular direction, resulting in configurations satisfying an incorrect energy condition. The former could also occur due to the lack of energy tolerance. That is not to say this method does not have its uses, as currently for large systems, an approximation method is useful. However, the differences can be quite large in the case of underestimation. To illustrate this, a rate constant using both methods will be reported.

The calculated IC rate constants using both the Lagrangian and LeCS methods for all systems are given in Table IV. At the Franck-Condon limit, the rate constants for the Polyacenes were found to be very small, with rates contants of 2.72×10^2 s^{-1}, 1.74×10^5 s^{-1}, and 1.06×10^4 s^{-1} for Anthracene, Tetracene, and Pentacene respectively. These rates are negligible, and as such clearly require a second order correction, yielding corrected rates of 3.69×10^6 s^{-1}, 2.60×10^7 s^{-1}, and 4.70×10^6 s^{-1} for Anthracene, Tetracene, and Pentacene respectively. Comparison of these rate constants to those published by Pedash and coworkers[9] show very agreeable results for Anthracene and Tetracene when considering second order processed. However for Pentacene, the rate constants here is too low. It is possible that due to the energetic proximity of electronic excited states, Pentacene may experience IC transferring to a higher energy state, but without explicit examination it is difficult to say. Nijegorodov and coworkers[14] noted a rate constant of 1.0×10^8 s^{-1} for Pentacene, but used the semiempirical formalism originally proposed by Plotnikov[24–26] which estimates part of the nuclear-vibrational coupling as a function of the number of hydrocarbon bonds along the molecule. It is possible that this method may intrinsically factor in second order processes. It is interesting to note that the linewidths of these three systems shrinks with respect to the number of aromatic rings, shifting from 0.11 PHz to 0.04 PHz. As these linewidths are computed from first principles, it is possible a semiempirical fix could push the rate constants higher in value.

For DPP, the IC rate constants were found to be 2.79×10^6 s^{-1} and 4.27×10^3 s^{-1} for the first and second order processes respectively, with a linewidth of 0.10 PHz. Here, we see that for DPP, second order processes are not very important for the IC mechanism. While this similar first order dominance would be expected for PDI, this is not the case here, with first and second order rates of 3.16×10^3 s^{-1} and 5.89×10^{10} s^{-1} respectively. PDI is well known to possess a near unity PLQY[92,93], which therefore infers small rate nonradiative rate constants. Here, the Franck-Condon rate constant is of an acceptable size, while the Herzberg-Teller term is grossly overestimated. This error is due to fact that our model found 5 high energy normal modes with non-zero HR factors. High energy modes have larger contributions to the Hessian, and therefore over-contribute to the rate constant. In the case of PDI, we found two modes with significant HR factors of energy larger than 0.4 eV, as per the Supplementary Information. Further examination of these high energy modes shows deformation of the outermost Hydrogens. This suggests the QC model used here does not treat these with sufficient accuracy. Therefore, application of a higher accuracy model would likely find these same normal modes either at a lower energy, or with smaller HR factors, circumventing this problem. Thinking about this in a physical sense, the high energy modes would have a very low probability of occupation, due to their thermal accessibility with respect to other lower energy modes. As such, modes above a certain energy threshold can be considered to have a negligible contribution to the IC rate constant. Following this argument, if you truncate the CS by culling all high energy modes; six modes ranging in energy from 0.398-0.442 eV, the total second order corrected IC rate constant for the $S_1 \rightarrow S_0$ transition using the Lagrangian method is found to be 3.3 s^{-1}. As such, we can

FIG. 3. Visualised rates for each chromophore with respect to CS Index at the Franck-Condon point.

expect an approximate LeCS second order corrected IC rate constant of somewhere between $10^3 - 10^4$ s^{-1}, following a comparison of other LeCS Vs. Lagrangian $k_{IC,HT}$ rate constants. Here we have taken to assuming a corrected rate constant of $k_{IC,HT} = 10^4$ s^{-1}. This issue is not observed in any other system.

It is worth highlighting that some of the rate constants predicted by the Lagrangian method overestimate the rates. Examination of the normal modes show minimal deformation between the ground and excited state geometries, further reflected by the existence of only a small number of TPMs with sizable HR factors. The Polyacenes possess a small number of TPMs, with a maximum of 24 participating modes in Pentacene, while DPP only shows 13 TPMs. In fact, PDI is the only system with a large number of TPMs, at 53. This is because the molecule only has one degree of symmetry due to a slight twist about the chromophore centre of mass. As such, only a very small number of occupations would contribute to

the rate of IC. Here, the Lagrangian method examines the continuous maximum rather than the discrete maximum, which is only viable for narrow distributions. In other words, the Lagrangian rate is actually artificially raised, with the acceptable configurations found with the Lagrangian CS theoretical maximum likely falling outside of the analytical LeCS. Direct comparison of LeCS rate constants to the Lagrangian rate constants show that use of the Lagrangian method alone yields varying results, with the best numbers being out of the range of the LeCS method by at minimum a factor of 2 and at most by three orders of magnitude. At a first order approximation, the rate is overestimated for Anthracene, Pentacene, and DPP, while it is grossly underestimated for Tetracene and PDI. Interestingly, this is different for the second order correction, as the Herzberg-Teller term effectively squares the differences, in addition to the influence of high energy modes in PDI as mentioned previously. Here, we generally see a gross underestimation of values, except for Pentacene, where the rate constant is overestimated, and falls much closer to what is expected in literature[9].

To understand why this over/underestimation happens, we can plot the results of the computed LeCS rate constants, as a function of the CS index, as shown in Figure 3. Beginning with the Polyacenes, these systems are relatively small with respect to the number of TPMs. For Anthracene, a $\mathscr{L}_{max}$ value of 16.67 was noted. As we cannot compute a fractional index, rounding up artificially raises the rate constant to 2.43×10^3 s^{-1}, in this case by an order of magnitude. For Tetracene, this has the opposite effect. Here, the $\mathscr{L}_{max}$ value is 13.19, resulting in a rate of 6.13×10^2 s^{-1} and an overall decrease by 3 orders of magnitude. In both these cases, it is clear that the rounding is too far in a given direction, resulting in configurations satisfying an incorrect energy condition. For Pentacene however, the error is minimized, as the $\mathscr{L}_{max}$ value of 5.78 is close to the natural maximum of the LeCS curve, resulting in a rate of 2.83×10^4 s^{-1}. In this case, the Lagrangian method can be considered reasonable. This is similar for DPP, whose $\mathscr{L}_{max}$ value of 12.78 yields a Lagrangian rate of 6.60×10^6 s^{-1}. Here, the spread of viable occupations along the CS is very large, suggesting the rate is being artificially increased again due to a displaced CS vector index. For PDI however, we see that the widened CS is grossly underestimated. Here, a large portion of the CS contributed to the overall rate constant, which goes against the Lagrangian approximation, resulting in a erroneous rate constant. For a such a large system to have only 5 TPMs with HR factors larger than 0.10, a very small rate is expected. In the case of a Lagrangian estimation, the larger number of TPMs result in a vast spread of satisfactory configurations, resulting in a Lagrangian rate constant underestimated by several orders of magnitude.

Recently, Valiev and co-workers[30] noted the importance of anharmonic effects to the overall IC rate constant. They found that by considering anharmonicity, the rate constant for Naphthalene increased by several orders of magnitude. While the addition of Herzberg-Teller effects solves for a lot of the error within the Franck-Condon regime, this suggests that the harmonic approximation itself may not be enough to explain the IC pathway for heavily mixed excited states. This is similarly concluded by Kohn and co-workers[94], who highlighted difficulties associated with the calculation of rate constants based on near-equilibrium energetics. Unfortunately, we have yet to implement the proposed formalism for rate constants within an anharmonic space. However, it is something we will do in the future.

TABLE V. Tabulated ISC rate constants for all studied chromophores. Transition rates are given for all triplet levels in close energetic proximity to, and those triplet levels lower in energy to the first singlet excited state. First and second order corrected rate constants are given in units of s^{-1}.

Compound	Transition	$k_{ISC,FC}$	$k_{ISC,FC+HT}$
Anthracene	$S_1 \rightsquigarrow T_1$	2.785×10^{-9}	3.904×10^{0}
	$S_1 \rightsquigarrow T_2$	1.507×10^{-1}	2.079×10^{8}
	$S_1 \rightsquigarrow T_3$	3.658×10^{-3}	7.959×10^{1}
Tetracene	$S_1 \rightsquigarrow T_1$	7.246×10^{-9}	1.366×10^{-1}
	$S_1 \rightsquigarrow T_2$	3.605×10^{-1}	2.366×10^{8}
Pentacene	$S_1 \rightsquigarrow T_1$	7.577×10^{-11}	1.116×10^{-2}
	$S_1 \rightsquigarrow T_2$	3.276×10^{-1}	2.622×10^{8}
DPP	$S_1 \rightsquigarrow T_1$	4.111×10^{2}	8.687×10^{6}
	$S_1 \rightsquigarrow T_2$	1.644×10^{0}	3.902×10^{7}
	$S_1 \rightsquigarrow T_3$	3.919×10^{2}	1.840×10^{6}
PDI	$S_1 \rightsquigarrow T_1$	7.297×10^{4}	9.164×10^{5}
	$S_1 \rightsquigarrow T_2$	8.959×10^{-1}	1.081×10^{5}

D. Inter-System Crossing

The calculated ISC rate constants at both first and second order approximations are shown in Table V. When considering only direct spin-orbit coupling, rate constants are generally very low in magnitude. Anthracene for example, yielded a combined first order rate constant of 1.51×10^{-1} s^{-1}, due entirely to the near-resonant $S_1 \rightarrow T_2$ transition, which is much too small to be realistic. Comparison of this rate to the total ISC rate calculated by Nijegorodov and co-workers[14] to be 1.51×10^7 s^{-1} shows that our yield is underestimated by several orders of magnitude. This is further confirmed by Parker & Joyce[95], who show a large ISC quantum yield of 0.70 in ethanol. This pattern of low first order rate constants is common across all of the studied chromophores, with combined first order rate constants of 3.61×10^{-1} s^{-1} and 3.28×10^{-1} s^{-1} for Tetracene and Pentacene. Moving to the more stable DPP and PDI chromophores, direct spin-orbit coupling is stronger, yielding combined first order rate constants of 8.05×10^2 s^{-1} and 7.30×10^4 s^{-1} respectively. For DPP, it is difficult to find literature rate constants to compare to, however it is clear that the tunability of the chromophore would also affect the singlet-triplet pathways. Similarly, PDI is also very tunable in its properties. However, PDI is well known to display a fluorescence quantum yield of close to unity, so a small ISC rate would therefore be expected.

While it is understandable that a number of these rate constants are low due to symmetry rules, it becomes clear

our spin-orbit coupling terms are being underestimated to some degree. Rate constants predicted using other methodologies[9,14,84] report much larger rates, suggesting direct spin-orbit coupling components lack the ability to completely predict the ISC rate constants. It is likely the underestimation is attributed to the lack of vibronic coupling components within the triplet wavefunctions. A number of the chromophores under investigation all possess tightly packed together electronic states, suggesting strong second order coupling between them. A similar phenomenon was observed by Tatchen et al.[15] for the Psoralene compound, with ISC rate constants being consistently underestimated using only direct spin-orbit coupling terms.

Second order corrections to the ISC rate constants yield much more positive results. For Anthracene, Tetracene, and Pentacene, we recorded overall second order corrected rate constants of 2.08×10^8 s^{-1}, 2.37×10^8 s^{-1}, and 2.62×10^8 s^{-1} respectively, all corresponding to the near-resonance of the $S_1 \rightarrow T_2$ transition. Here, especially for ISC rates, we highlight the importance of second order processes, which allow for ultrafast pathways despite minimal direct coupling factors. While these values are faster than those reported by Nijegorodov and coworkers[14], they do agree well with those published by Pedash and coworkers[9] who did consider higher order processes, of 1.90×10^8 s^{-1}, and 2.50×10^8 s^{-1} for Anthracene and Tetracene. Interestingly, they note an almost non-existent ISC rate constant for Pentacene, attributing all non-radiative decay to the IC mechanism. Here, Nijegorodov and coworkers[14] agree, arguing an IC quantum yield of 0.75 for the chromophore.

For DPP, the combined second order corrected ISC rate constant is much more evenly distributed across all low lying triplet levels, yielding a total of 4.95×10^7 s^{-1}. With nothing to compare to, it is difficult to speculate as to whether this is correct or not, but as the rate is slower than the radiative rate constant, this suggests the chromophore will possess an efficient quantum yield. Finally, PDI yielded a total second order corrected ISC rate constant of 9.16×10^5 s^{-1}, with a 90% contribution from the $S_1 \rightarrow T_1$ transition. This is in reasonable agreement with the expected properties of PDI as proposed by Isukapalli and coworkers[84], who implemented strict symmetry conditions whereby this transition is forbidden, unlike here. However they are low with respect to the radiative rate, and as such can be considered respectable.

E. Internal Fluorescence Quantum Yield

Computed PLQYs are tabulated in Table VI. Here, first order PLQYs are seen to be generally overestimated, due to the omission of higher order photophysical properties found in compounds with complex mixing of excited state wavefunction components. For Anthracene, Tetracene, and Pentacene, quantum yields are all values of unity to near-unity, with PLQYs of 1.00, 0.99, and 1.00 respectively. Similar results were noted for DPP and PDI, with PLQYs of 0.98 and 1.00 respectively. While for PDI, this is a positive result, for the other chromophores adhering to only first order rate constants is not accurate enough.

TABLE VI. Computed internal quantum yield values using only first order rate constants (FC), and second order corrected rate constants (FC+HT), compared to those found in literature.

Q_D	Anthracene	Tetracene	Pentacene	DPP	PDI
$Q_{D,FC}$	1.00	0.99	1.00	0.98	1.00
$Q_{D,FC+HT}$	0.19	0.08	0.04	0.70	0.99
Lit	0.24[a]	0.21[a]	0.08[a]	0.4-0.9[b]	0.97[c]

[a]From Ref. 14 using Cyclohexane. [b]From Ref. 44 using various solvents. [c]From Ref. 92 using Toluene.

When we begin to consider second order corrections to the PLQYs, the results are much more positive. For the Polyacenes, the second order corrected PLQYs are 0.19, 0.08, and 0.04 respectively, which compares quite well to the literature values of 0.24, 0.21, and 0.08 reported by Nijegorodov and coworkers experimentally in Cyclohexane[14]. For Anthracene, we obtain a PLQY of 0.19, which finds an excellent agreement with experiment. The interesting cases are for Tetracene and Pentacene. In both cases, we see a lower than normal PLQY due to a large ISC rate constant for the near resonant $S_1 \rightarrow T_2$ pathway. However, we know this is not necessarily the case as per Table I. We can therefore conclude that the triplet equilibrium geometries are not accurate within the TDDFT methodology. Despite this, the resulting quantum yields are within an acceptable margin of error.

Second order corrected PLQYs for DPP and PDI yield efficiencies of 0.70 and 0.99 respectively. In the case of the former, this falls well within the expected region of 0.4-0.9 reported by Auwalu & Cheng[44]. In the case of the latter however, while this does compare well with the expected value of 0.97 as reported by Yang and coworkers[92], the efficacy of this result is dependant on how you view the truncation of high energy TPMs. Due to the two high energy normal modes with non-zero HR factors, the second order rate constant was overestimated by several orders of magnitude, calculated at 5.885×10^{10} s^{-1}. However, upon removing these TPMs from the CS, a new second order rate constant of 10^4 s^{-1} can be estimated within the LeCS framework, yielding PLQYs of near unity or 0. While physically, this is a sound correction, it would be worth repeating these calculations, on the same or similar systems, at higher levels of theory such as MRMP, CC2, or CASPT2 to be certain of accurate geometries, TPMs, and NACME terms between the ground and first singlet excited states. That being said, these results suggest the methodology is sound with respect to the level of theory in which quantum chemical parameters are computed.

V. CONCLUSIONS

Here, we have presented a versatile methodology for the computation of various rate constants in order to model the PLQY of any given chromophore monomer without the use of any semi-empirical parameters; entirely at a first principles level. At a quantum chemical level, we found that the com-

puted singlet properties yielded accurate energies and configuration state functions with respect to what was previously reported in the literature. However, it was noted that in the triplet manifold, while configuration state functions agreed well, the energies of the equilibrium minima did not. In particular, all the Polyacenes were noted to display a near resonance condition for the $S_1 \rightarrow T_2$ pathway, foreshadowing that some ISC rate constants may be overestimated. Radiative processes were found to agree well with similar studies reported in literature, showing that our approximation for second order normalisation could accurately estimate the full transition dipole moment for chromophores where Herzberg-Teller processes are not dominant. Consequentially, each computed fluorescence lifetime was found to be within an acceptable margin of error to the cited literature values.

Following to non-radiative processes, the IC rate constants at the Franck-Condon limit were shown to be smaller than expected. Application of a second order correction yielded much more appreicable rate constants, closer to those reported in the literature. For the Polyacenes, we noted a shrinking of the linewidth with respect to the number of aromatic rings in the chromophore, which could leave room for improvement if using a semiempirical value for the linewidth, artificially raising the IC rate constants. For DPP, we noted that second order processes did not play an important role in the spin-conserved pathways. For PDI, we noted an ultrafast mechanism under the Herzberg-Teller regime initially. However, removal of high energy TPMs from the CS resulted in an appreciable rate constant. Here we also highlighted the differences between the Lagrangian method and LeCS method of computing bosonic configurations, as there was always a disagreement between the two methods. Explicit explanations were given as to why they did not agree, highlighting that the Lagrangian method, while very useful as a tool to estimate very large systems that cannot be fully solved in a reasonable amount of time, consistently results in errors of up to 3 orders of magnitude. In fact, it was only found to display reasonable rates in the case of Pentacene, where the predicted maximum as close to the actual maximum. Computed ISC rate constants were found to be almost negligible at the Franck-Condon point, but became much more appreciable upon a second order correction. Interestingly, we found that for Pentacene the dominant mechanism is ISC, which disagrees strongly with the literature. Finally, the first order PLQYs were shown to be generally overestimated, with all values close to unity, but were once again made to look much more attractive upon implementation of a second order correction, yielding PLQYs of 0.19, 0.08, 0.04, 0.70, and 0.99 for Anthracene, Tetracene, Pentacene, DPP, and PDI respectively. As such, we are confident the methodology presented here is viable for use in the field of quantum chemistry. However, as with all quantum chemisty, care needs to be taken with respect to the accuracy of geometries and consequential excited state energies.

In conclusion, the presented model was able to predict the PLQYs and corresponding rate constants from first principles various chromophores to a reasonable degree. With a clear path forward, the proposed model has a future in the role of property prediction. A small number of weaknesses were noted, such as difficulties in accurately replicating experimental environments and the errors noted in computation of triplet chemical properties at the TDDFT level of theory. However, viable solutions to each issue were presented and discussed, such as the recomputation at higher levels of theory, an anharmonic treatment of vibronic coupling for both the IC and ISC rate, and the explicit computation of radiative processes as opposed to the approximation. Once these problems are dealt with, the next step would be to push towards intermolecular decay processes and even larger systems.

VI. SUPPLEMENTARY INFORMATION

SI includes the following for each studied chromophore: visualised frontier orbitals, tabulated electronic structure properties of all important electronic excited states (plus one additional state) for all equilibrium geometries of interest, optimised cartesian coordinates for all geometries, energies and corresponding HR factors for all TPMs for each $S_1 \rightarrow S_0$ transition, and an explanation as to how derivative terms are treated.

VII. ACKNOWLEDGEMENTS

This work was supported by the Australian Government through the Australian Research Council (ARC) under the Centre of Excellence scheme (project number CE170100026). This work was also supported by computational resources provided by the Australian Government through the National Computational Infrastructure National Facility and the Pawsey Supercomputer Centre. A special thanks to Dr. Siobhan Bradley, for her most welcome insight into the DPP chromophore.

VIII. DATA AVAILABILITY

The data that supports the findings of this study are available within the article [and its supplementary material].

IX. REFERENCES

[1] I. Lyskov, M. Etinski, C. M. Marian, and S. P. Russo, J Mater Chem C **6**, 6860 (2018).
[2] E. Mouedden, *Lifetime and efficiency improvement of organic luminescent solar concentrators for photovoltaic applications.*, Master's thesis, Edith Cowan University (2016).
[3] V. Lemaur, M. Steel, D. Beljonne, J.-L. Brédas, and J. Cornil, J Am Chem Soc **127**, 6077 (2005).
[4] J. L. Banal, B. Zhang, D. J. Jones, K. P. Ghiggino, and W. W. H. Wong, Acc Chem Res **50**, 49 (2016).
[5] B. Zhang, H. Soleimaninejad, D. J. Jones, J. M. White, K. P. Ghiggino, T. A. Smith, and W. W. H. Wong, Chem Mater **29**, 8395 (2017).
[6] B. Zhang, I. Lyskov, L. J. Wilson, R. P. Sabatini, A. Manian, H. Soleimaninejad, J. M. White, T. A. Smith, G. Lakhwani, D. J. Jones, K. P. Ghiggino, S. P. Russo, and W. W. H. Wong, J Mater Chem C **8**, 8953 (2020).

[7]N. Meftahi, A. Manian, A. J. Christofferson, I. Lyskov, and S. P. Russo, J. Chem. Phys. **153**, 064108 (2020).
[8]J. Birks, J. Res. Natl. Bur. Stand. A. Phys. Chem. **80A**, 389 (1976).
[9]Y. Pedash, O. Prezhdo, S. Kotelevskiy, and V. Prezhdo, J. Mol. Struct. **585**, 49 (2002).
[10]J. Franck and E. G. Dymond, Trans Faraday Soc **21**, 536 (1926).
[11]E. Condon, Phys Rev **28**, 1182 (1926).
[12]E. U. Condon, Phys Rev **32**, 858 (1928).
[13]E. Herzberg, G. & Teller, Z. Phys. Chem (Leipz.) **21**, 410 (1933).
[14]N. Nijegorodov, V. Ramachandran, and D. Winkoun, SPECTROCHIM ACTA A **53**, 1813 (1997).
[15]J. Tatchen, N. Gilka, and C. M. Marian, Phys Chem Chem Phys **9**, 5209 (2007).
[16]Z. E. X. Dance, S. M. Mickley, T. M. Wilson, A. B. Ricks, A. M. Scott, M. A. Ratner, and M. R. Wasielewski, J Phys Chem A **112**, 4194 (2008).
[17]M. Etinski, J. Tatchen, and C. M. Marian, J Chem Phys **134**, 154105 (2011).
[18]J. Tatchen and C. M. Marian, Phys Chem Chem Phys **8**, 2133 (2006).
[19]Y. Bai, J. Rawson, S. A. Roget, J.-H. Olivier, J. Lin, P. Zhang, D. N. Beratan, and M. J. Therien, Chem Sci **8**, 5889 (2017).
[20]T. J. A. Wolf, R. H. Myhre, J. P. Cryan, S. Coriani, R. J. Squibb, A. Battistoni, N. Berrah, C. Bostedt, P. Bucksbaum, G. Coslovich, R. Feifel, K. J. Gaffney, J. Grilj, T. J. Martinez, S. Miyabe, S. P. Moeller, M. Mucke, A. Natan, R. Obaid, T. Osipov, O. Plekan, S. Wang, H. Koch, and M. Gühr, Nat Commun **8**, 10.1038/s41467-017-00069-7 (2017).
[21]K. L. Litvinenko, N. M. Webber, and S. R. Meech, J Phys Chem A **107**, 2616 (2003).
[22]L. G. Samsonova, N. I. Selivanov, T. N. Kopylova, V. Y. Artyukhov, G. V. Maier, V. G. Plotnikov, V. A. Sazhnikov, A. A. Khlebunov, and M. V. Alfimov, High Energy Chem **43**, 105 (2009).
[23]M. Bracker, C. M. Marian, and M. Kleinschmidt, The Journal of Chemical Physics **155**, 014102 (2021).
[24]V. G. Plotnikov and B. A. Dolgikh, Opt Spectrosc+ **43**, 522 (1977).
[25]Plotnikov, Solid State Phys (1973).
[26]V. G. Plotnikov, Int J Quantum Chem **16**, 527 (1979).
[27]G. V. Maier, V. Y. Artyukhov, and N. R. Rib, Russ Phys J **36**, 949 (1993).
[28]R. R. Valiev, V. N. Cherepanov, G. V. Baryshnikov, and D. Sundholm, Phys Chem Chem Phys **20**, 6121 (2018).
[29]G. V. Baryshnikov, R. R. Valiev, V. N. Cherepanov, N. N. Karaush-Karmazin, V. A. Minaeva, B. F. Minaev, and H. Ågren, Phys Chem Chem Phys **21**, 9246 (2019).
[30]R. R. Valiev, R. T. Nasibullin, V. N. Cherepanov, G. V. Baryshnikov, D. Sundholm, H. Ågren, B. F. Minaev, and T. Kurtén, Phys. Chem. Chem. Phys. **22**, 22314 (2020).
[31]H. Kellerer, U. Pferschy, and D. Pisinger, in *Knapsack Problems* (Springer Berlin Heidelberg, 2004) pp. 483–493.
[32]R. A. Shaw, A. Manian, I. Lyskov, and S. P. Russo, J Chem Phys **154**, 084102 (2021).
[33]S. Banerjee, A. Baiardi, J. Bloino, and V. Barone, J Chem Theory Comput **12**, 774 (2016).
[34]M. K. Kretov, A. V. Scherbinin, and N. F. Stepanov, Russ J Phys Chem A+ **87**, 245 (2013).
[35]P. V. Yurenev, M. K. Kretov, A. V. Scherbinin, and N. F. Stepanov, J Phys Chem A **114**, 12804 (2010).
[36]M. Kleinschmidt, J. Tatchen, and C. M. Marian, J Chem Phys **124**, 124101 (2006).
[37]M. Kleinschmidt, J. Tatchen, and C. M. Marian, J Comput Chem **23**, 824 (2002).
[38]D. Biermann and W. Schmidt, J Am Chem Soc **102**, 3163 (1980).
[39]Y. Kawashima, T. Hashimoto, H. Nakano, and K. Hirao, Theor Chem Acc **102**, 49 (1999).
[40]Y. H. Meyer, R. Astier, and J. M. Leclercq, J Chem Phys **56**, 801 (1972).
[41]L. E. A. Suarez, M. F. S. J. Menger, and S. Faraji, Mol Phys **118**, e1769870 (2020).
[42]J. Burgos, M. Pope, C. E. Swenberg, and R. R. Alfano, Physica Status Solidi (b) **83**, 249 (1977).
[43]S. Qu and H. Tian, Chem Commun **48**, 3039 (2012).
[44]M. A. Auwalu and S. Cheng, Chemosensors **9**, 44 (2021).
[45]R. S. Szabadai, J. Roth-Barton, K. P. Ghiggino, J. M. White, and D. J. D. Wilson, Aust J Chem **67**, 1330 (2014).
[46]M. Grzybowski and D. T. Gryko, Adv Opt Mater **3**, 280 (2015).
[47]A. B. Pun, L. M. Campos, and D. N. Congreve, J Am Chem Soc **141**, 3777 (2019).
[48]A. D. Becke, J Chem Phys **98**, 5648 (1993).
[49]A. Schäfer, C. Huber, and R. Ahlrichs, J Chem Phys **100**, 5829 (1994).
[50]M. J. Frisch, G. W. Trucks, H. B. Schlegel, G. E. Scuseria, M. A. Robb, J. R. Cheeseman, G. Scalmani, V. Barone, G. A. Petersson, H. Nakatsuji, X. Li, M. Caricato, A. V. Marenich, J. Bloino, B. G. Janesko, R. Gomperts, B. Mennucci, H. P. Hratchian, J. V. Ortiz, A. F. Izmaylov, J. L. Sonnenberg, D. Williams-Young, F. Ding, F. Lipparini, F. Egidi, J. Goings, B. Peng, A. Petrone, T. Henderson, D. Ranasinghe, V. G. Zakrzewski, J. Gao, N. Rega, G. Zheng, W. Liang, M. Hada, M. Ehara, K. Toyota, R. Fukuda, J. Hasegawa, M. Ishida, T. Nakajima, Y. Honda, O. Kitao, H. Nakai, T. Vreven, K. Throssell, J. A. Montgomery, Jr., J. E. Peralta, F. Ogliaro, M. J. Bearpark, J. J. Heyd, E. N. Brothers, K. N. Kudin, V. N. Staroverov, T. A. Keith, R. Kobayashi, J. Normand, K. Raghavachari, A. P. Rendell, J. C. Burant, S. S. Iyengar, J. Tomasi, M. Cossi, J. M. Millam, M. Klene, C. Adamo, R. Cammi, J. W. Ochterski, R. L. Martin, K. Morokuma, O. Farkas, J. B. Foresman, and D. J. Fox, Gaussian16 Revision B.01 (2016), gaussian Inc. Wallingford CT.
[51]S. J. Bradley, M. Chi, J. M. White, C. R. Hall, L. Goerigk, T. A. Smith, and K. P. Ghiggino, Phys. Chem. Chem. Phys. **23**, 9357 (2021).
[52]W. Chen, Z. Dai, H. Liu, H. Liu, Y. Shi, and X. Li, J. Lumin. **168**, 192 (2015).
[53]I. Lyskov, M. Kleinschmidt, and C. M. Marian, J Chem Phys **144**, 034104 (2016).
[54]A. D. Becke, Phys Rev A **38**, 3098 (1988).
[55]U. of Karlsruhe, TURBOMOLE V7.3 2018, a development of University of Karlsruhe and Forschungszentrum Karlsruhe GmbH, TURBOMOLE GmbH, since 2007; (1989-2007).
[56]A. Schäfer, A. Klamt, D. Sattel, J. C. W. Lohrenz, and F. Eckert, Phys Chem Chem Phys **2**, 2187 (2000).
[57]M. Kleinschmidt and C. M. Marian, Chem Phys **311**, 71 (2005).
[58]F. Plasser, S. Gómez, M. F. S. J. Menger, S. Mai, and L. González, Physical Chemistry Chemical Physics **21**, 57 (2019).
[59]H. B. Klevens and J. R. Platt, J Chem Phys **17**, 470 (1949).
[60]S. Sambursky and G. Wolfsohn, Trans. Faraday Soc. **35**, 427 (1940).
[61]I. B. Berlman, *Handbook of Fluorescence Spectra of Aromatic Molecules* (Elsevier, 1971).
[62]J. Ferguson, L. W. Reeves, and W. G. Schneider, Can J Chem **35**, 1117 (1957).
[63]M. K. Orloff, J Chem Phys **47**, 235 (1967).
[64]M. Baba, M. Saitoh, K. Taguma, K. Shinohara, K. Yoshida, Y. Semba, S. Kasahara, N. Nakayama, H. Goto, T. Ishimoto, and U. Nagashima, J. Chem. Phys. **130**, 134315 (2009).
[65]R. Rüger, T. Niehaus, E. van Lenthe, T. Heine, and L. Visscher, J Chem Phys **145**, 184102 (2016).
[66]R. P. Steiner and J. Michl, J Am Chem Soc **100**, 6861 (1978).
[67]S. Murov, *Handbook of photochemistry* (M. Dekker, New York, 1993).
[68]G. N. Lewis and M. Kasha, J Am Chem Soc **66**, 2100 (1944).
[69]R. Pariser, J Chem Phys **24**, 250 (1956).
[70]J. J. Burdett, A. M. Müller, D. Gosztola, and C. J. Bardeen, The Journal of Chemical Physics **133**, 144506 (2010).
[71]C. M. Marian and N. Gilka, J. Chem. Theory Comput. **4**, 1501 (2008).
[72]P. M. Zimmerman, F. Bell, D. Casanova, and M. Head-Gordon, J. Am. Chem. Soc. **133**, 19944 (2011).
[73]Y. Tomkiewicz, R. P. Groff, and P. Avakian, J Chem Phys **54**, 4504 (1971).
[74]A. Amirav, U. Even, and J. Jortner, J. Phys. Chem. **85**, 309 (1981).
[75]E. Heinecke, D. Hartmann, R. Müller, and A. Hese, J. Chem. Phys. **109**, 906 (1998).
[76]M. Banasiewicz, I. Deperasińska, and B. Kozankiewicz, J. Phys. Chem. A **107**, 662 (2003).
[77]P. M. Zimmerman, Z. Zhang, and C. B. Musgrave, Nat Chem **2**, 648 (2010).
[78]P. B. Coto, S. Sharifzadeh, J. B. Neaton, and M. Thoss, J Chem Theory Comput **11**, 147 (2014).
[79]T. Baruah, A. Garnica, M. Paggen, L. Basurto, and R. R. Zope, J Chem Phys **144**, 144304 (2016).
[80]P. E. Hartnett, E. A. Margulies, C. M. Mauck, S. A. Miller, Y. Wu, Y.-L. Wu, T. J. Marks, and M. R. Wasielewski, J. Phys. Chem. B. **120**, 1357 (2016).
[81]F. Zhang, Y. Ma, Y. Chi, H. Yu, Y. Li, T. Jiang, X. Wei, and J. Shi, Sci Rep **8**, 8208 (2018).

[82]G. Hinze, R. Métivier, F. Nolde, K. Müllen, and T. Basché, J. Chem. Phys. **128**, 124516 (2008).
[83]L. Yang and S. J. Jang, J Chem Phys **153**, 144305 (2020).
[84]S. V. K. Isukapalli, R. S. Lekshmi, P. K. Samanta, and S. R. Vennapusa, J Chem Phys **153**, 124301 (2020).
[85]Y. Kurashige and T. Yanai, Bull Chem Soc Jpn **87**, 1071 (2014).
[86]M. Kaur and D. H. Choi, Chem Soc Rev **44**, 58 (2015).
[87]C. Ye, J. Zhang, X. Lin, T. Zhang, B. Wang, and T. He, Opt Mater Express **7**, 3529 (2017).
[88]Y. Y. Pan, J. Huang, Z. M. Wang, D. W. Yu, B. Yang, and Y. G. Ma, RSC Advances **7**, 26697 (2017).
[89]J. M. Dixon, M. Taniguchi, and J. S. Lindsey, Photochemistry and Photobiology **81**, 212 (2005).
[90]M. Kirkus, L. Wang, S. Mothy, D. Beljonne, J. Cornil, R. A. J. Janssen, and S. C. J. Meskers, J Phys Chem A **116**, 7927 (2012).
[91]T. Xiong, R. Włodarczyk, and P. Saalfrank, Chem Phys **515**, 728 (2018).
[92]S. I. Yang, S. Prathapan, M. A. Miller, J. Seth, D. F. Bocian, J. S. Lindsey, and D. Holten, J. Phys. Chem. B **105**, 8249 (2001).
[93]W. E. Ford and P. V. Kamat, J. Phys. Chem. **91**, 6373 (1987).
[94]A. W. Kohn, Z. Lin, and T. V. Voorhis, J. Phys. Chem. C. **123**, 15394 (2019).
[95]C. A. Parker and T. A. Joyce, Trans Faraday Soc **62**, 2785 (1966).

Anthracene

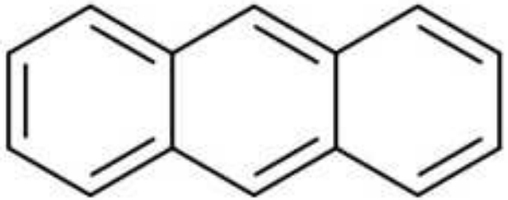

Tetracene

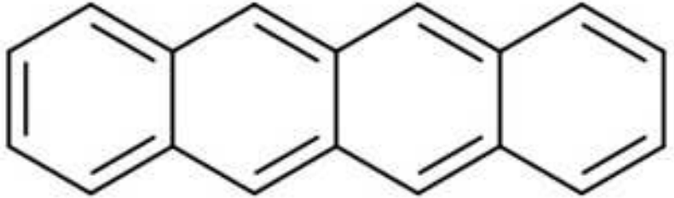

Pentacene

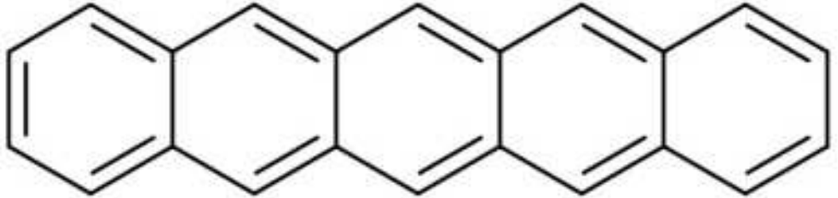

DPP

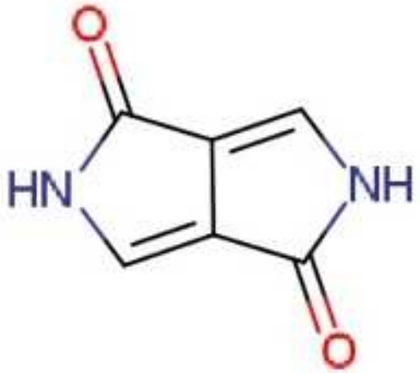

PDI

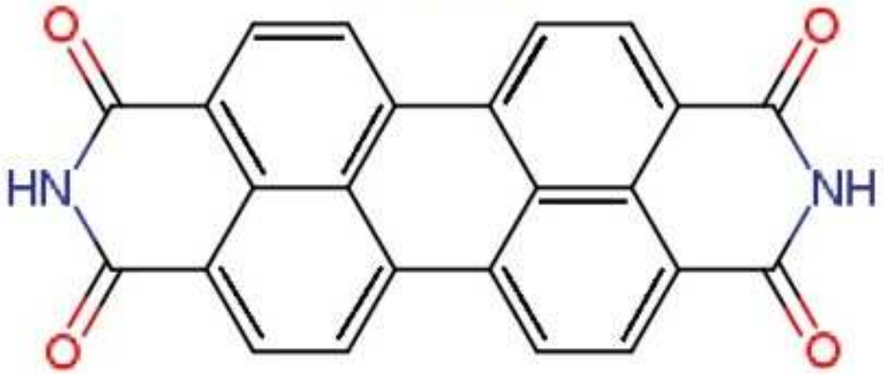

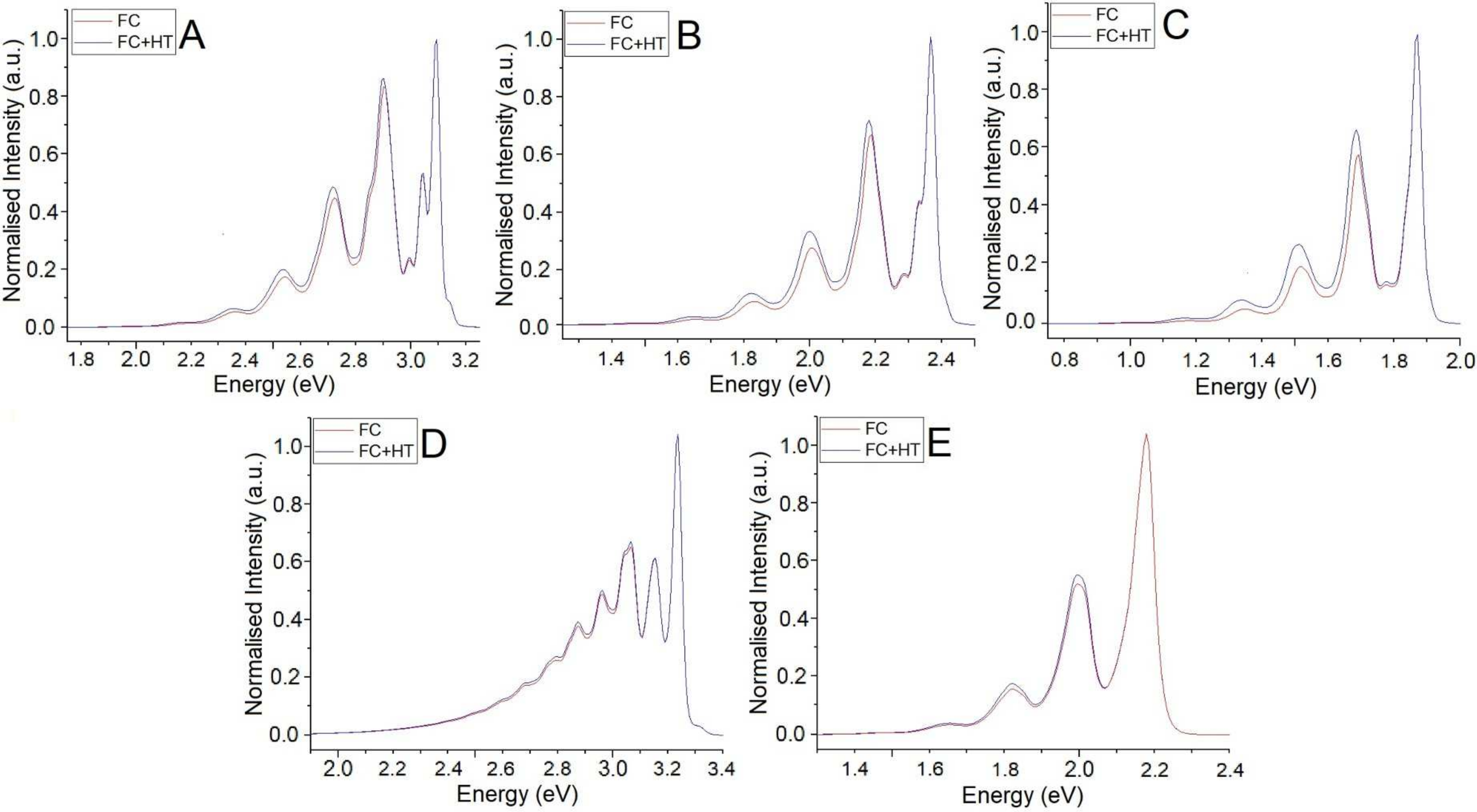
A
FC
FC+HT
Normalised Intensity (a.u.)
Energy (eV)
B
C
D
E

Anthracene

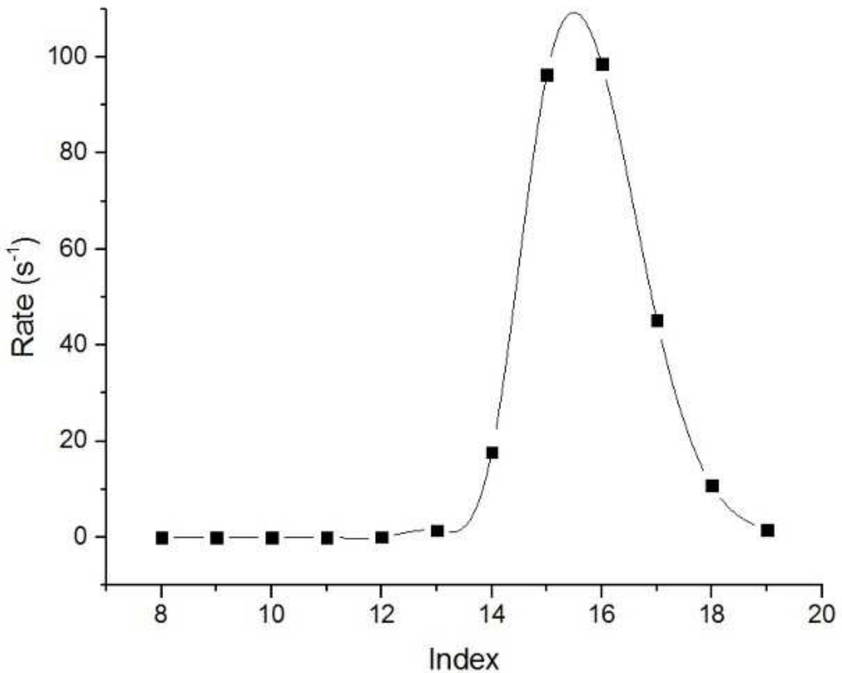

Tetracene

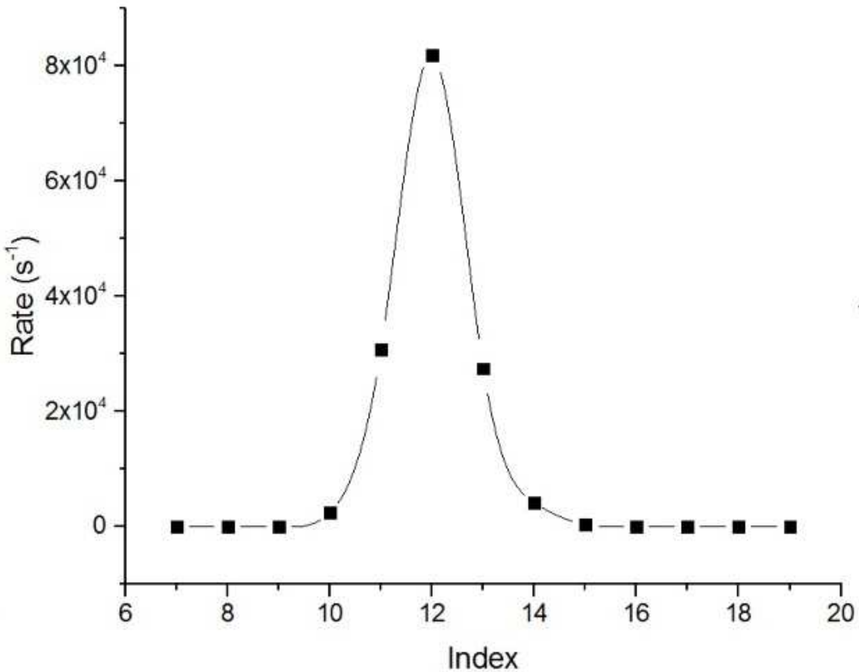

Pentacene

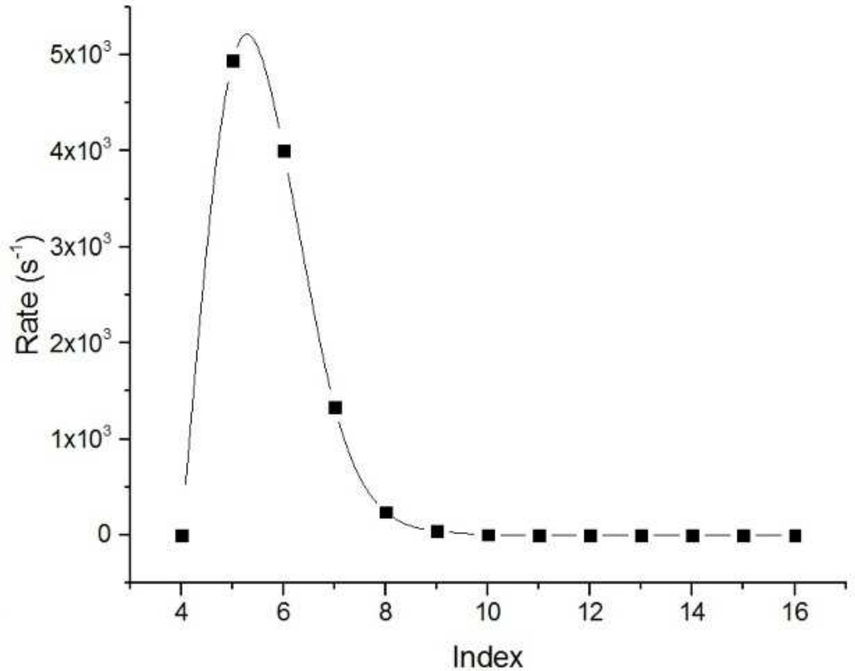

DPP

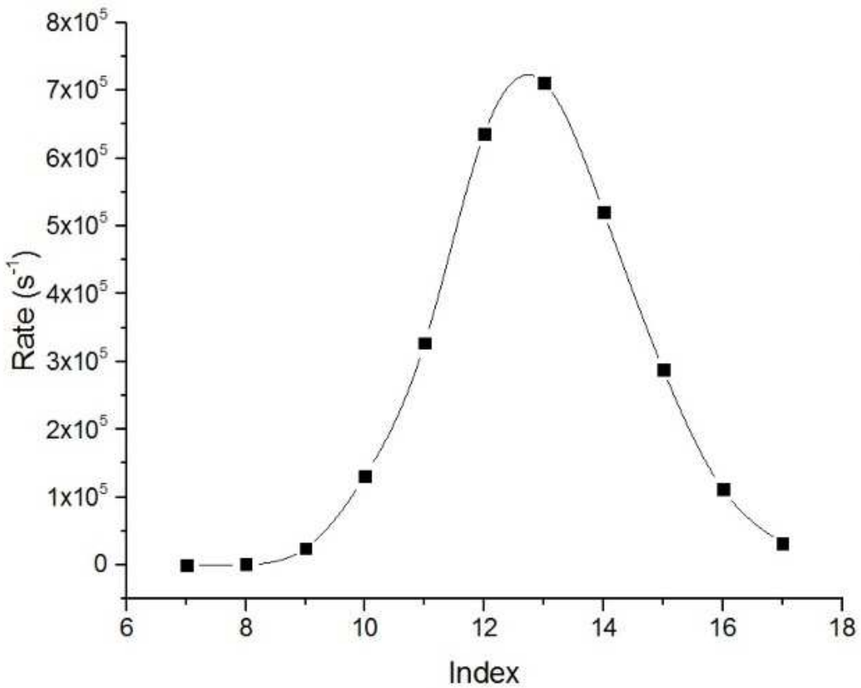

PDI